Published in final edited form as:
Chem Sci. 2013 February 1; 4(2): 655–663. doi:10.1039/C2SC21502K.

Resistive-pulse measurements with nanopipettes: detection of Au nanoparticles and nanoparticle-bound anti-peanut IgY†

Yixian Wang[a], **Kaan Kececi**[a,‡], **Michael V. Mirkin**[a], **Vigneshwaran Mani**[b], **Naimish Sardesai**[b], and **James F. Rusling**[b,c,d]

Michael V. Mirkin: mmirkin@qc.cuny.edu; James F. Rusling: James.Rusling@uconn.edu

[a]Department of Chemistry and Biochemistry, Queens College–CUNY, Flushing, New York 11367, USA. Fax: +1 7189975531; Tel: +1 7189974111 [b]Department of Chemistry, U-60, University of Connecticut, 55 N. Eagleville Rd., Storrs, CT 06269-3060, USA. Fax: +1 860-486-2981; Tel: +1 860-486-4909 [c]Department of Cell Biology, University of Connecticut Health Center, Farmington, CT, USA [d]School of Chemistry, National University of Ireland at Galway, Ireland

Abstract

Solid-state nanopores have been widely employed in sensing applications from Coulter counters to DNA sequencing devices. The analytical signal in such experiments is the change in ionic current flowing through the orifice caused by the large molecule or nanoparticle translocation through the pore. Conceptually similar nanopipette-based sensors can offer several advantages including the ease of fabrication and small physical size essential for local measurements and experiments in small spaces. This paper describes the first evaluation of nanopipettes with well characterized geometry for resistive-pulse sensing of Au nanoparticles (AuNP), nanoparticles coated with an allergen epitope peptide layer, and AuNP–peptide particles with bound antipeanut antibodies (IgY) on the peptide layer. The label-free signal produced by IgY-conjugated particles was strikingly different from those obtained with other analytes, thus suggesting the possibility of selective and sensitive resistive-pulse sensing of antibodies.

Introduction

A family of sensing devices based on measurement of the ion current flowing through a microscopic aperture includes solid-state nanopores,[1] artificial ion channels,[2] and carbon nanotubes. [3] The ability to detect single particles that can enter a microscopic pore and partially block the current is common to all these devices, known as resistive-pulse sensors. A number of sensing schemes employing these devices have been developed and used for DNA detection and sequencing,[4] studies of transport processes at the level of single molecules,[5] ion-selective sensing,[6] detecting single molecules,[1c,7] biosensing,[1a,3b,8] and single ion-channel recording.[9] Various types of nanopores have been employed for resistive-pulse sensing,[10] which is conceptually similar to the classical Coulter counter. The advantages of resistive-pulse biosensing are widely recognized. The recorded current pulses are single-molecule (or single-particle) events; hence the possibility of the ultralow detection limit.[3,7,11]

†Electronic supplementary information (ESI) available. See DOI: 10.1039/c2sc21502k

Correspondence to: Michael V. Mirkin, mmirkin@qc.cuny.edu; James F. Rusling, James.Rusling@uconn.edu.
‡Present address: Department of Chemistry, Istanbul Medeniyet University, Kadikoy, Istanbul, Turkey.

In this article, we develop new approaches to quantitative resistive-pulse sensing with nanopipettes and demonstrate the use of nanopipette-based sensors for selective detection of antibodies to peanut allergens (IgY).[12] Peanut and tree nut allergy related symptoms affect ~1% of all Americans.[13] Peanut allergens are glycoproteins that elicit immune responses elevating IgE antibody levels in the human body. *Arachis hypogaea* glycoprotein peanut allergens Ara h1, Ara h2, and Ara h3 are the major glycoprotein allergens that elicit specific IgE response (sIgE) due to epitopes of protein in allergic patients.[14a] Peptide sequence of Ara h1 induces specific IgE levels that can be measured in serum and that may aid in detecting the likelihood of severe allergy episodes. Ara h2 is an abundant glycoprotein present in nuts, and is considered the most potent peanut allergen that is most frequently recognized by specific IgE from allergic individuals.[14] Here, we used the Ara h 2-2 peptide sequence for detection of anti-peanut chicken IgY, a model antibody for human IgEs with a similar 3-D structure.[15] Ara h 2-2 peptide-modified gold nanoparticles were employed to capture IgY offline from solution for detection using a nanopipette-based sensor.

In resistive-pulse sensing,[10] a detectable particle—or a biomolecule—must be sufficiently small to pass through the pore orifice, but at the same time large enough to cause a measurable change in the recorded ion current, Δi. In most cases, $\Delta i < 0$; however, increases in apparent conductivity of the pore during the translocation event have also been reported.[16] Individual blocking events on the millisecond or sub-millisecond time scale can be recorded using a patch clamp amplifier or a similar device.

Nanopipettes are similar to nanopores in having a nanometer- sized orifice that can sense the analyte species entering and partially blocking the aperture.[17] The ion current (i_0) is driven by voltage applied between two reference electrodes placed inside and outside of the nanopipette (Fig. 1A). A nanopipette offers several important advantages including the ease of fabrication, small physical size (the outer diameter of the pipette tip can be as small as ≤10 nm),[18] and the needle-like geometry, which makes it suitable as a probe for scanning probe microscopies.[17,19–22] Few applications of nanopipettes to resistive- pulse sensing have been reported,[11,23] and methodology for characterizing the inside geometry of a pipette, which is essential for such measurements, has yet to be developed. The two main geometric parameters are the pipette radius (a) and the pipette angle (θ; Fig. 1B), which define the shape of the narrow tapered shaft adjacent to its tip and therefore largely determine the ion current and the pipette resistance. Here we show that pipette geometry can be characterized by combining resistive-pulse experiments with steady-state voltammetry of ion transfer across the interface between two immiscible electrolyte solutions (ITIES). Then, we use a model system of gold nanoparticles (AuNP), AuNP–peptide allergen and AuNP–peptide allergen particles that have bound IgYs to demonstrate the use of nanopipettes for label-free detection of antibodies.

Results and discussion

Size distribution and zeta (ζ)-potentials of particles

TEM images of different particles used in our experiments are shown in Fig. 2, and related size distributions are given in Fig. 3. After drying on TEM grids, the particles showed considerable aggregation. To determine the size, we focused on individually isolated particles. The image of commercial citrate-stabilized AuNP (Fig. 2A) and the corresponding size distribution (Fig. 3A) show an average diameter of 9.5 ± 0.3 nm in a good agreement with the 10 nm nominal particle size given by the manufacturer. In solution, these particles also tend to aggregate, as confirmed by preliminary light scattering experiments. After modification of AuNP with mercaptohexadecanoic acid (MHDA), the average particle diameter (9.6 ± 0.3 nm) remained nearly the same (Fig. 2B and 3B) which is consistent since the organic layer is not visible in TEM. AuNP–peptide and AuNP–peptide–IgY were stained

with 0.5% phosphotungstic acid so that their surface layers could be visualized. Here, particles with no aggregation and a larger diameter than the AuNP–peptide were specifically sought out for imaging so that we could characterize the sizes of particles assumed to be AuNP–peptide–IgY. Significant aggregation on the TEM grids did not allow counting of different particle types. The somewhat larger diameter of AuNP–peptide particles (13.9 ± 0.8 nm; Fig. 2C and 3C) corresponds to the thickness of a peptide monolayer (~4.5 nm). The peptide film appears as a white halo around each particle in Fig. 2C. The halos around AuNP–peptide–IgY in Fig. 2D are thicker and less uniform in agreement with the larger average diameter (15.1 ± 1.4 nm) and higher polydispersity (Fig. 2D and 3D) of these particles. (Control experiments confirmed that the halos were not produced by phosphotungstic acid itself. TEM images of Au nanoparticles pretreated with PTA with neither peptide nor antibodies attached to them exhibited no halo (Fig. 2E).)

Zeta potentials were measured for the same four types of particles (Table 1). The highest negative value (−52 mV) was obtained for citrate-stabilized AuNPs, while AuNP–MHDA in the presence of Tween-20 exhibited a very small value −4.9 mV. Without Tween-20, the ζ-potential of AuNP–MHDA was somewhat higher (−18 mV), but the surfactant had to be added to avoid aggregation of these particles. The ζ-potential of AuNP–peptide–IgY was slightly less negative than that of AuNP–peptide.

Characterization of nanopipettes

The pipette radius was determined from voltammetry at the ITIES performed in the following cell:

$$\underset{DCE}{\mathrm{Ag|10\,mM\,THATPB+1\,mM\,TBACIO_4||15\,mM\,NaCl}}\underset{pipette}{\mathrm{|Agcl|Ag}} \quad (1)$$

Fig. 4 shows a typical voltammogram for perchlorate transfer across a water–1,2-dichloroethane (DCE) interface formed at the tip of a quartz nanopipette. With a non-silanized pipette, the diffusion limiting current follows eqn (2):[24]

$$i_d = 3.35\pi zFDac \quad (2)$$

where F is the Faraday constant, c, D and z are the concentration, diffusion coefficient, and charge of the transferred ion, respectively, and a is the pipette radius. With $D = 8 \times 10^{-6}$ cm^2 s^{-1} measured for ClO_4^- in DCE using larger (*i.e.*, micrometer-sized) pipettes, $a = 25$ nm was calculated from Fig. 4 using eqn (2).

The pipette angle, θ can be determined in two different ways—from resistance measurements[25a] and by common ion voltammetry.[25b, c] The pipette resistance was found from the current–voltage (i–V) curves recorded in aqueous solution containing 15 mM NaCl and 10 mM phosphate buffer (PB; the same solution was used in our resistive-pulse experiments). With a relatively large nanopipette (*e.g.*, a > ~100 nm; Fig. 5A), the i–V curves were essentially linear, and the total resistance, R, could be extracted from the slope. i–V curves obtained with smaller pipettes were non-linear because of current rectification (Fig. 5B);[26] whereas an essentially linear part of such a curve recorded at low applied voltages (*e.g.*, ±20 mV; the inset in Fig. 5B) was used for determining R. The total pipette resistance comprises two components, $R = R_{int} + R_{ext}$, *i.e.*, the resistances of the inner and outer solutions. Assuming that the pipette orifice is disk-shaped, R_{ext} is entirely determined by its radius and solution conductivity (κ), $R_{ext} = 1/(4\kappa a)$.[27] θ was evaluated from the internal pipette resistance ($R_{int} = R - R_{ext}$) using a simple analytical approximation[25a]

$$R_{\text{int}} = 1/\kappa\pi a \tan\theta \quad (3)$$

The conductivity of 0.1 M KCl is 1.29 Ω^{-1} m^{-1}, while that of the buffer solution (15 mM NaCl + 10 mM PB) is 0.294 Ω^{-1} m^{-1}, which was measured by comparing the resistance of these two solutions obtained with the same large pipettes (3 to 20 μm radius). The geometric parameters and resistances found for several pipettes are summarized in Table 2.

These geometric parameters were used to evaluate the suitability of a given pipette for detecting particles with a specific radius, r_p. The question here is what relative change in ion current ($\Delta i/i_0$) and translocation time (τ, *i.e.*, the width at half pulse height) can be expected when such a particle enters a pipette with the radius a and angle θ? To our knowledge, no theory is available in the literature for particle translocation through the pipette tip. Comprehensive numerical modeling of the translocation of spherical particles through conical-shaped nanopores was reported recently.[28] However, the model in ref. 28 did not include electroosmosis, which was found to be insignificant because of high particle mobility. In our case, the effect of electroosmosis may be more important (see below) and especially difficult to model exactly. Instead, we modified the approximate analytical model previously developed for a spherical particle translocation through a conical nanopore[7] and its slightly refined version,[29] in which the shape of the current pulse was calculated. Unlike the treatments in ref. 7 and 29, we used the measurable θ value instead of the radius of the larger pore orifice, which is not available for a nanopipette (see ESI†). Another important difference is that we determined a independently from ITIES voltammetry rather than calculated from pipette resistance. Although this simplified model does not take into account electroosmosis, NP interactions with glass surface, and double-layer effects, it is suitable for predicting the magnitude of a current pulse and for semi-quantitative analysis of its shape and duration.

The current–time pulses were calculated for the translocation of nanoparticles through pipettes with different a and θ values as shown in Fig. 6. Although, the radius of the transferable particle has to be smaller than that of the pipette, the larger the r_p/a the larger the change in pipette resistance and hence $\Delta i/i_0$ (Fig. 6A). For a given r_p/a, the larger the θ the larger the resistive-pulse signal, as shown in Fig. 6B. Using 15 mM NaCl + 10 mM PB solution, the range of i_0 in our experiments (below) typically was 100 pA < i_0 < 1 nA, depending on a and the applied voltage. With a typical level of noise in our experiments of ~1 pA and the required signal/noise ratio of ≥3, the smallest detectible $\Delta i_{max}/i_0$ is on the order of 0.01. From Fig. 6A, one can see that a pipette with the radius a and a typical θ value of 10° must be suitable for the detection of particles with $a/2 \le r_p < a$. Particles with $a/4 < r_p < a/2$ may be harder to detect (this depends on the i_0 value); and particles with $r_p \le a/4$ are almost certainly undetectable. The lower limit for r_p/a is significantly higher with θ=5°, and lower with θ=15° (Fig. 6B). By adjusting the pulling program, the pipettes with suitable geometry were fabricated and characterized before resistive-pulse experiments.

Translocation of citrate-stabilized Au nanoparticles (AuNP)

The translocation of citrate-stabilized AuNP was used as a model system to explore basic features of current pulses obtained with nanopipettes. Fig. 7A shows a typical current–time recording for the translocation of 10 nm AuNPs through a 28 nm-diameter pipette. Unlike a background trace I obtained with no nanoparticles added to the external solution, a number of pulses with the current changes much larger than the noise level can be seen in trace II. With the r_p/a value close to 1/3, $\Delta i/i_0$ is expected to be ~0.01. Thus, smaller current

†Electronic supplementary information (ESI) available. See DOI: 10.1039/c2sc21502k

blockages correspond to the translocation of individual AuNPs, while larger spikes are likely to be produced by the particle dimers, which are sufficiently small to penetrate through the 28 nm pipette orifice.

Trace II in Fig. 7A is a part of a series of recordings (the total recording time was 12 min) from which the average spike density was found to be ~0.5 events per s. The comparison of this number to the diffusional flux of AuNPs to the pipette orifice can provide information about the rate-determining step of the overall translocation process. The consecutive steps of this process are the transport of particles to the pipette orifice in the external solution, the ingress of particles into the pipette, and the transport inside the narrow shaft of the pipette. The diffusional flux of electrically neutral particles to the pipette orifice is given by eqn (4)

$$\text{flux} = xD_p c_p a \quad (4)$$

where x is a function of r_g/a (r_g is the outer wall radius in Fig. 1B; $r_g/a \approx 1.5$ for a typical glass or quartz pipette,[20] corresponding to $x \approx 5$); D_p and c_p are the diffusion coefficient and concentration of AuNPs, respectively. Although AuNPs are negatively charged, the contribution of migration to their flux in the external solution should be small because of a high concentration of supporting electrolyte in solution and a nm-range pipette radius,[30] and the flux of charged particles can still be evaluated from eqn (4). In Fig. 7A, $c_p = 1.2 \times 10^{12}$ particles per cm^3, $a = 14$ nm, and $D_p \approx 2 \times 10^{-7}$ cm^2 s^{-1} can be estimated for a 10 nm-diameter particle from the Stokes–Einstein equation at 20 °C. The resulting flux is ~2 particles per s, which is consistent with the 0.5 events per s extracted from the experimental data. Better agreement can be achieved if one takes into account the finite size of a AuNP, which is comparable to the radius of the pipette aperture. Unlike an ion or a small molecule, which can enter the much larger pipette anywhere within its orifice, a nanoparticle has to come in sufficiently close to the pipette center to avoid the collision with the outer wall. For example, in Fig. 7A (trace II), a 10 nm-diameter spherical AuNP could enter the 28 nm pipette only if the radial distance between the particle center and the pipette center was ≤9 nm (otherwise, the particle would hit the pipette wall instead of getting inside). Therefore, the apparent orifice radius available for the particle ingress is only 9 nm, and this value (rather than $a = 14$ nm) should be substituted in eqn (4), yielding the flux value of ~1 particle per s. (Although this number is reasonably close to the experimentally found frequency of blockages, the presented analysis is not strictly quantitative because of the size polydispersity of AuNPs; *cf.* Fig. 3. Another factor that may have decreased the observed frequency of translocations is the possibility of a NP being bounced back after partially penetrating into the pipette.) In contrast, the average pulse duration in the same set of data was ~1 ms, suggesting that ~1000 particles per second could translocate through the pipette if their transport inside the pipette rather than diffusion in the external solution were the rate limiting step (see ESI† for the discussion of the blockage duration).

It is important to note that current blockages by AuNPs were observed only when a positive potential (*e.g.*, +150 mV in Fig. 7A) was applied to the reference electrode inside the pipette with respect to the external reference. This indicates that the translocation of negatively charged AuNP is driven by electrophoresis rather than simple diffusion of particles through the pipette narrow shaft or electroosmosis. Moreover, the direction of the electroosmotic flow in this case was opposite to that of the electrophoresis.

Translocation of peptide-modified gold nanoparticles

The nanopipette methodology was used to develop a resistive-pulse sensing platform for the detection of antipeanut allergen antibodies. To attain selective detection of IgY, peptide modified 10 nm gold nanoparticles (AuNP–peptide) were prepared using a two-step process,

as described in the Experimental section. Trace II in Fig. 7B shows an example of a current–time recording obtained with AuNP–peptide. The frequency of spikes was 1.2 events per s for 1.8 nM AuNP–peptide, that is similar to ~1.7 particles per s value estimated from diffusion flux [eqn (4)]. As discussed above, a better agreement can be achieved by correcting for the finite particle size. The spikes in Fig. 7B are more uniform that those in Fig. 7A because Au–peptide dimer particles are too large to penetrate a 32 nm pipette orifice. Similarly to bare AuNP, the translocation of AuNP–peptide is driven by electrophoresis. Trace III in Fig. 7B was recorded at V=−100 mV. No current pulses were found, indicating that no AuNP–peptide particle transfer at a negative potential.

Pipettes with different diameters were used to detect the polydispersity of Au–peptide particles due to their crosslinking by peptide molecules. Fig. 8 shows scatter plots of AuNP–peptide translocation experiments with three different pipettes (rows 1, 3 and 5 in Table 2). As discussed above, only single Au–peptide particles (rather than dimers or other aggregates) can enter either 22 nm or 28 nm-diameter pipette. The $\Delta i_{max}/i_0$ for a given pipette is largely determined by the r_p/a value (see ESI† for more details). Since both pipettes probed the same collection of Au–peptide particles (with the size distribution given by Fig. 3C), it is intuitive that the extent of blockage should be larger for a smaller pipette. Accordingly, $\Delta i_{max}/i_0$ values ranged from 0.023 to 0.156 for the 22 nm pipette (circles) and from 0.006 to 0.045 for the 28 nm pipette (diamonds). The possibility of sizing nanoparticles by resistive-pulse measurements with nanopores based on the relationship between the blockage magnitude and particle size was shown recently.[31] Here, the particle diameter ranges extracted from the recordings obtained with two pipettes are somewhat different, *i.e.*, from 9.4 nm to 17.9 nm (28 nm pipette; mean NP diameter, 13.8 nm) and 12.4 nm to 19.7 nm (22 nm pipette, mean NP diameter, 16.1 nm). By comparing with the particle size shown in Fig. 3, those particles could be bare Au (9.5 nm), Au–MHDA (9.6 nm) or Au–peptide (13.9 nm) or Au dimers (19.0 nm). The average pulse width was longer for the 22 nm pipette (1.06 ms) than for the 28 nm pipette (0.82 ms) because of the smaller applied voltage (200 mV *vs.* 300 mV) and larger r_p/a; the latter factor was especially significant for particle diameters larger than ~15 nm.

Two scatter plots obtained with a much larger pipette (108 nm-diameter; triangles) are totally different from other data in Fig. 8. This pipette was too large to detect single AuNP–peptide species, so the recorded pulses must be due to dimers and other aggregates. The $\Delta i_{max}/i_0$ values range from 0.004 to 0.027, which correspond to the particle diameters between 29.6 nm and 56.0 nm, according to the developed theory (ESI† and Fig. 6). As expected, there is no significant difference between the average magnitude of current blockages in the recordings obtained with this pipette at 800 mV (purple) and 900 mV (orange); however the mean pulse width is larger at a lower applied voltage (4.9 ms *vs.* 3.5 ms), further indicating that the translocation was driven by electrophoresis. Despite higher applied voltage, the translocation of particle aggregates was slower than that of single AuNP–peptide monitored by smaller pipettes.

Translocation of AuNP–peptide–IgY

The current–time recordings for AuNP–peptide–IgY translocations (Fig. 9) are completely different from the aforementioned data. In contrast to the current blockages observed at positive potentials in Fig. 7A and B, with AuNP–peptide–IgY the current pulses were found only at negative potentials applied to the inner reference electrode (*e.g.*, −200 mV in Fig. 9B), and the direction of the pulse was reversed from that of the other particles. We observed this behavior using several pipettes of different diameters, AuNP–peptide–IgY from two different batches, and different pH values (7.0 and 9.5; data for pH 9.5 not shown). Since the ζ-potential of AuNP–peptide–IgY is negative, the translocation of these particles at negative voltages indicates that electroosmosis dominates over electrophoresis, and the

translocation direction is electroosmotic. One reason for this difference is a less negative ζ-potential of AuNP–peptide–IgY as compared to AuNP–peptide and AuNP (Table 1). Even with bare AuNPs, the electroosmosis significantly affected the particle transport inside the pipette, resulting in a lower effective mobility. As demonstrated by Firnkes *et al.*,[32] the translocation direction of protein molecules through nanopores is determined by the difference of ζ-potentials, $\Delta\zeta = \zeta_{particle} - \zeta_{pore}$, which in ref. 32 was ~10 mV. The change in the voltage sign between AuNP–peptide–IgY and AuNP–peptide (ζ_{pore} was the same for both particles, and the $\zeta_{particle}$ of AuNP–peptide– IgY is 7 mV less negative) is qualitatively in line with the results in ref. 32. Quantitative analysis of this phenomenon is difficult because of the complicated structure of AuNP–peptide–IgY, and additional factors (*e.g.,* nonuniform charge distribution on the particle) should also contribute to it along with the ζ-potential value.

The resistive pulses produced by AuNP–peptide–IgY translocation that reflect increases in the absolute value of the ion current is a striking feature, as opposed to the current decrease in Fig. 7A and B. Positive Δi have previously been observed in resistive-pulse experiments, and the increase in current during the translocation event was attributed to the charge on the particle itself[16a] and the motion of the counterions.[16b] In the present case of antibody detection, the change in direction of the current pulse and the change in voltage sign when antibody is bound to the particle is an analytical advantage, and the AuNPs with bound IgY should be readily distinguishable from those without IgY. These major differences between current pulses produced by antibody-conjugated particles and either bare Au or Au–peptide nanoparticles confirmed the feasibility of selective resistive-pulse sensing of antibodies with nanopipettes. Importantly, the recordings obtained with AuNP– peptide showed no current pulses at negative applied voltages (trace III in Fig. 7B), indicating that the spikes in Fig. 9 can only be attributed to AuNP–peptide–IgY.

Shapes of current pulses

Representative current pulses obtained with different types of particles are shown in Fig. 10. Asymmetrical spikes with the sharp initial decrease in current followed by a slow relaxation (“tail”) were most often observed with both AuNP–peptide (Fig. 10A) and Au–MHDA (Fig. 10B). The pipette resistance, which is largely determined by that of its tapered narrow shaft, increases sharply when the particle enters the pipette and then decreases slowly. This kind of pulses were previously shown to give good fits to simulated data[28] and approximate theory developed for electrophoretic transport in the nanopores.[29] Using an approximate model for a nanopipette (see ESI†), a good fit between the theory and the experimental pulses was obtained in Fig. 10B with a single adjustable parameter, effective mobility (μ). Notice however that $\mu = 1.8 \times 10^{-10} m^2\ V^{-1}\ s^{-1}$ obtained from the fit is at least an order of magnitude lower than the electrophoretic mobilities measured previously for similarly sized particles. This would be consistent with an extremely low value of ζ-potential (<1 mV). This finding points to the significant effect of the electroosmotic flow, whose direction is opposite to that of the electrophoresis, resulting in the diminished value of the effective mobility.[32]

Bipolar pulses with a larger magnitude negative peak ($\Delta i < 0$) and a small positive spike (Fig. 10C) were also observed with both AuNP and AuNP–peptide. Such pulses previously reported in the literature, have been recently simulated for the nanopore translocation.[33] The peak width of positive ($\Delta i > 0$) pulses obtained with AuNP–peptide–IgY varied from relatively short (~1 ms) to quite long (~10 ms; Fig. 10D), which may be due to the combination of the slow electroosmotic flow and stronger interactions of IgY-modified particles with the pipette wall. Our understanding of the conductivity enhancement mechanism is incomplete because of the complicated structure of AuNP–peptide–IgY and

difficulties in describing its interactions with the nanopipette surface. A more sophisticated model is needed for quantitative analysis of the pulse shape in this case.

Conclusions

We developed nanometer-sized pipettes as a platform for resistive-pulse sensing. Thorough characterization of the pipette size and geometry helps establish the relationship between the particle size and the expected pulse magnitude for a given pipette. The correspondence between frequency of the recorded single particle events and the diffusion current of particles to the orifice suggests the possibility of quantitative determination of analyte species in solution.

The new nanopipette-based approach was used for label-free detection of peptide-modified particles and antibodies attached to them. The possibility of probing mixtures of differently sized analytes was also revealed. The current pulses produced by antibody-conjugated particles and either bare Au or Au–peptide nanoparticles occurred at different translocation voltages (positive for AuNP and AuNP–peptide *vs.* negative for AuNP–peptide–IgY) and exhibited opposite signs of Δi. These major differences are essential for selective resistive-pulse sensing of antibodies with nanopipettes. If this behavior is common to other protein-modified nanoparticles, the developed sensing platform can be useful for detecting other types of antibodies and protein biomarkers.

In most reported resistive-pulse experiments, selective detection of biomolecules was achieved by functionalizing the nanopore (*e.g.*, by immobilizing antibodies on its surface[11b]). In our study, the analyte (IgY) was selectively captured offline using peptide modified gold nanoparticles. After the analyte capture, the particles can be washed to remove potential interferences and avoid complex mixtures.[34] In this way, selective resistive-pulse sensing of biomolecules can be attained using simple glass or quartz pipettes without laborious surface modification procedures. This approach can also help to avoid other experimental issues that hinder resistive-pulse sensing in biological media, such as clogging and non-specific adsorption of proteins.

Experimental

Chemicals and materials

The following chemicals were used as received: sodium chloride, 1,2-dichloroethane (DCE), *N*-hydroxysuccinimide (NHS), mercaptohexadecanoic acid (16-MHDA), 1-(3-(dimethylamino)-propyl)-3-ethylcarbodiimide hydrochloride (EDC), and sodium tetraphenylborate (NaTPB) from Sigma-Aldrich; monosodium phosphate and disodium phosphate from J.T. Baker Chemical; tetrahexylammonium chloride (THACl) and tetrabutylammonium perchlorate ($TBAClO_4$) from Fluka. Tetrahexylammonium tetraphenylborate (THATPB) was prepared by metathesis of NaTPB with THACl and recrystallized from acetone. Aqueous solutions were prepared from deionized water (Milli-Q, Millipore Co.). 10 mM sodium phosphate buffer (PB) solution at pH 7.0 either with or without 1.8 mg mL^{-1} Tween-20 was prepared and used for surface modification of gold colloids.

Citrate-stabilized, 10 nm diameter (as specified by the vendor) Au nanoparticles (5.7×10^{12} particles per mL, *i.e.*, ~9.5 nM) were purchased from Ted-Pella Inc. The stock solution was diluted to the desired concentration in 15 mM NaCl + 10 mM PB. Affinity-purified chicken antipeanut antibodies (IgY) were from Immunology Consultants Laboratory Inc. Peptide fragment of Ara h 2-2 (H_2N-QSPSYPDREYSDEDRQIKQMLHQECPRL-$CONH_2$) was synthesized by Anaspec Inc.

Preparation of gold AuNPs modified with 16-MHDA (AuNP– MHDA)

Gold colloids were modified with 16-MHDA according to previously reported procedures.[35] Briefly, 1400 μL of 10 nM gold colloid (Ted-Pella Inc) was centrifuged at 13 000 rpm for 90 min. The resultant gold colloid pellet was then reconstituted in 400 μL of deionized water. Equal volume of 10 mM pH 7.0 PB with Tween-20 (PB-T) was added to the AuNP solution and allowed to incubate for 30 min. Then, 400 μL of degassed 0.5 mM ethanol solution of 16-MHDA was added and allowed to incubate for 3 h. Next, the nanoparticle solution was centrifuged for 2 h at 13 000 rpm. The resultant pellet was then washed with PB-T four times, reconstituted in 400 μL of PB-T, and stored at 4 °C. The prepared stock solution concentration was 22 nM, as determined by UV-V is spectroscopy (not shown).

Surface conjugation of Ara h 2-2 peptide to AuNP–MHDA

A peptide sequence with active amine functional group was conjugated to carboxylated gold nanoparticles by EDC–NHS amine coupling.[36] Briefly, 200 μL of AuNP–MHDA solution was centrifuged at 13 000 rpm for 25 min, the resultant nanoparticle pellet was reacted with 100 mM and 50 mM EDC–NHS in 10 mM pH 7.0 PB for 10 min to activate carboxyl groups on AuNPs. After the activation, the particles were washed with PB twice, and 360 μL of PB and 40 μL of 0.5 mg mL^{-1} Arah 2-2 peptide was added to the washed pellet and incubated for 30 min. Centrifugation and washing steps were performed thrice to remove any unbound peptide, and AuNP–peptide conjugate was subsequently reconstituted in 200 μL of PB. The stock solution produced in this way contained 22 nM AuNP–peptide.

IgY capture by AuNP–peptide

Different concentrations of IgY were allowed to react with AuNP–peptide conjugate to form AuNP–peptide–IgY. Typically, 200 μL of AuNP–peptide in 520 μL of PB was allowed to react with 80 μL of 1 ng mL^{-1} IgY in PB for 60 min in a small centrifuge tube using a mixer. For TEM, 100 ng mL^{-1} IgY was used. The obtained AuNP–peptide–IgY were then separated by centrifugation at 13 000 rpm for 2 min and washed with PB.

Characterization of transferrable particles

Transmission electron microscopy (TEM) was used to characterize the size distribution of particles. TEM was performed with Tecnai TEM at 80 kV accelerating voltage (340 000× magnification). The TEM grids were glow discharged in plasma cleaner (model PDC-32 G, from Harrick Plasma) prior to mounting samples on the carbon type-A grid (Ted Pella, Inc). Glow discharge treatment of TEM grids with air removes adsorbed hydrocarbons and makes a TEM grid carbon film surface negatively charged (hydrophilic), which allows aqueous solutions to spread easily. Samples (3 μL) were placed on carbon grids and dried under air for a 30 min. The samples were Au colloids (2× diluted, pH 7.0), MHDA AuNP (10× diluted, pH 7), Au–peptide (3.5× diluted, borate buffer pH 9.5), Au–peptide–IgY (100 ng mL^{-1}) (borate buffer pH 9.5). The sample grids were washed several times with deionized water to wash off the buffer. To negatively stain peptides and proteins, 0.5% phosphotungstic acid was added on the Au–peptide and Au–peptide–IgY sample grids and allowed to adsorb for 1 min, followed by several washings to wash off unadsorbed stain.

The stability and modification of gold nanoparticles were monitored using zeta potential analysis. Zeta potential measurements of modified Au nanoparticles were performed using ZetaPlus Zeta potential analyzer (Brookhaven Instruments Corporation, Holtsville, NY). The reported zeta potential values were obtained by averaging 5 readings.

Nanopipette preparation and voltammetry at the ITIES

Borosilicate or quartz capillaries (o.d./i.d. ratio of 1.0/0.58 and 1.0/0.70, respectively; Sutter Instrument Co., Novato, CA) were cleaned in piranha solution (3: 1 H_2SO_4–H_2O_2, v/v; **caution!** *this solution is a very strong oxidizing agent and very dangerous to handle in the laboratory. Protective equipment including gloves, goggles, and face shields should be used at all times*), rinsed with copious amount of deionized water and kept in furnace over-night. Nanopipettes were fabricated by pulling cleaned capillaries with a laser-based pipette puller (P-2000, Sutter Instrument Co.).[18a,20] Representative pulling parameters for pulling quartz capillaries are HEAT =760, FILAMENT =4, VELOCITY =29, DELAY =140, PULL =168.

The pulled pipettes were backfilled with aqueous solution containing 10 mM PB and 15 mM NaCl using a 10 μL syringe and immersed in 1,2-dichloroethane (DCE) solution containing 1 mM $TBAClO_4$. A 0.25 mm silver wire coated with AgCl was inserted into each pipette from the back. A two-electrode setup was employed with another 0.25 mm Ag wire serving as an organic reference electrode. Steady-state voltammograms were obtained using a BAS 100B/W electrochemical workstation (Bioanalytical Systems, West Lafayette, IN).

Resistive-pulse experiments

The pipette filled with 15 mM NaCl and 10 mM PB was dipped into the same aqueous solution containing nanoparticles of interest. A Multiclamp 700B amplifier (Molecular Devices Corporation, CA) was used in the voltage-clamp mode to apply voltage between the Ag/AgCl reference electrode inside the nanopipette and the external Ag/AgCl reference facing the pipette orifice and to measure the resulting current. The signal was digitized using a Digidata 1440A analog-to-digital converter (Molecular Devices) at a sampling frequency of 100 kHz. A low pass filter with 1–10 kHz bandwidth was used. The recordings with higher filter frequency, *e.g.*, 20 kHz, as well as with no filtering were obtained in control experiments to verify that shorter current pulses have not been missed or filtered out. The data were recorded and analyzed using pClamp 10 (Molecular Devices).

Supplementary Material

Refer to Web version on PubMed Central for supplementary material.

Acknowledgments

This work was financially supported by the National Science Foundation (CHE-0957313 and CBET-1251232; MVM) and by grant EB014586 from the National Institute of Biomedical Imaging and Bioengineering (NIBIB), NIH (JFR).

Notes and references

1. (a) Sexton LT, Horne LP, Martin CR. Mol BioSyst. 2007; 3:667. [PubMed: 17882330] (b) Griffiths J. Anal Chem. 2008; 80:23. [PubMed: 18052345] (c) Howorka S, Siwy Z. Chem Soc Rev. 2009; 38:2360. [PubMed: 19623355]
2. (a) Kasianowicz JJ, Brandin E, Branton D, Deamer DW. Proc Natl Acad Sci U S A. 1996; 93:13770. [PubMed: 8943010] (b) Bayley H, Cremer PS. Nature. 2001; 413:226. [PubMed: 11557992] (c) Majd S, Yusko EC, Billeh YN, Macrae MX, Yang J, Mayer M. Curr Opin Biotechnol. 2010; 21:439. [PubMed: 20561776]
3. (a) Ito T, Sun L, Henriquez RR, Crooks RM. Acc Chem Res. 2004; 37:937. [PubMed: 15609985] (b) Choi Y, Baker LA, Hillebrenner H, Martin CR. Phys Chem Chem Phys. 2006; 8:4976. [PubMed: 17091150]
4. Branton D, Deamer DW, Marziali A, Bayley H, Benner SA, Butler T, Di Ventra M, Garaj S, Hibbs A, Huang X, Jovanovich SB, Krstic PS, Lindsay S, Ling XS, Mastrangelo CH, Meller A, Oliver JS,

Pershin YV, Ramsey JM, Riehn R, Soni GV, Tabard-Cossa V, Wanunu M, Wiggin M, Schloss JA. Nat Biotechnol. 2008; 26:1146. [PubMed: 18846088]

5. (a) Fan R, Karnik R, Yue M, Li D, Majumdar A, Yang P. Nano Lett. 2005; 5:1633. [PubMed: 16159197] (b) Gershow M, Golovchenko JA. Nat Nanotechnol. 2007; 2:775. [PubMed: 18654430] (c) Kowalczyk SW, Kapinos L, Blosser TR, Magalhães T, van Nies P, Lim RYH, Dekker C. Nat Nanotechnol. 2011; 6:433. [PubMed: 21685911]
6. (a) Shim JH, Kim J, Cha GS, Nam H, White RJ, White HS. Anal Chem. 2007; 79:3568. [PubMed: 17411008] (b) Song C, Corry B. J Phys Chem B. 2009; 113:7642. [PubMed: 19419185]
7. Heins EA, Siwy ZS, Baker LA, Martin CR. Nano Lett. 2005; 5:1824. [PubMed: 16159231]
8. Martin CR, Siwy ZS. Science. 2007; 317:331. [PubMed: 17641190]
9. (a) White RJ, Ervin EN, Yang T, Chen X, Daniel S, Cremer PS, White HS. J Am Chem Soc. 2007; 129:11766. [PubMed: 17784758] (b) Schibel AEP, Edwards T, Kawano R, Lan W, White HS. Anal Chem. 2010; 82:7259. [PubMed: 20684522]
10. Bayley H, Martin CR. Chem Rev. 2000; 100:2575. [PubMed: 11749296]
11. (a) Karhanek M, Kemp JT, Pourmand N, Davis RW, Webb CD. Nano Lett. 2005; 5:403. [PubMed: 15794633] (b) Umehara S, Karhanek M, Davis RW, Pourmand N. Proc Natl Acad Sci U S A. 2009; 106:4611. [PubMed: 19264962]
12. Liu H, Malhotra R, Peczuh MW, Rusling JF. Anal Chem. 2010; 82:5865. [PubMed: 20540504]
13. Shreffler SH, Munoz-Furlong A, Sampson HA. J Allergy Clin Immunol. 2003; 112:1203. [PubMed: 14657884]
14. (a) Koppelman SJ, Wensing M, Ertmann M, Knulst AC, Knol EF. Clin Exp Allergy. 2004; 34:583. [PubMed: 15080811] (b) Shreffler WG, Lencer DA, Bardina L, Sampson HA. J Allergy Clin Immunol. 2005; 116:893. [PubMed: 16210066]
15. Warr GW, Magor KE, Higgins DA. Immunol Today. 1995; 16:392. [PubMed: 7546196]
16. (a) Chang H, Kosari F, Andreadakis G, Alam MA, Vasmatzis G, Bashir R. Nano Lett. 2004; 4:1551.(b) Smeets RMM, Keyser UF, Krapf D, Wu MY, Dekker NH, Dekker C. Nano Lett. 2006; 6:89. [PubMed: 16402793]
17. Morris C, Friedman AK, Baker LA. Analyst. 2010; 135:2190. [PubMed: 20563341]
18. (a) Shao Y, Mirkin MV. J Am Chem Soc. 1997; 119:8103.(b) Li Q, Xie S, Liang Z, Meng X, Liu S, Girault HH, Shao Y. Angew Chem, Int Ed. 2009; 48:8010.
19. Hansma PK, Drake B, Marti O, Gould SAC, Prater CB. Science. 1989; 243:641. [PubMed: 2464851]
20. Cai CX, Tong YH, Mirkin MV. J Phys Chem B. 2004; 108:17872.
21. (a) Comstock DJ, Elam JW, Pellin MJ, Hersam MC. Anal Chem. 2010; 82:1270. [PubMed: 20073475] (b) Takahashi Y, Shevchuk AI, Novak P, Murakami Y, Shiku H, Korchev YE, Matsue T. J Am Chem Soc. 2010; 132:10118. [PubMed: 20590117]
22. (a) Snowden ME, Güell AG, Lai SCS, McKelvey K, Ebejer N, O'Connell MA, Colburn AW, Unwin PR. Anal Chem. 2012; 84:2483. [PubMed: 22279955] (b) Güell AG, Ebejer N, Snowden ME, McKelvey K, Macpherson JV, Unwin PR. Proc Natl Acad Sci U S A. 2012; 109:11487. [PubMed: 22635266]
23. Gao C, Ding S, Tan Q, Gu L-Q. Anal Chem. 2009; 81:80. [PubMed: 19061410]
24. Beattie PD, Delay A, Girault HH. J Electroanal Chem. 1995; 380:167.
25. (a) Laforge FO, Carpino J, Rotenberg SA, Mirkin MV. Proc Natl Acad Sci U S A. 2007; 104:11895. [PubMed: 17620612] (b) Rodgers PJ, Amemiya S. Anal Chem. 2007; 79:9276. [PubMed: 18004818] (c) Rodgers PJ, Amemiya S, Wang Y, Mirkin MV. Anal Chem. 2010; 82:84. [PubMed: 20000448]
26. (a) Wei C, Bard AJ, Feldberg SW. Anal Chem. 1997; 69:4627.(b) White HS, Bund A. Langmuir. 2008; 14:2212. [PubMed: 18225931] (c) Guerrette JP, Zhang B. J Am Chem Soc. 2010; 132:17088. [PubMed: 21073197] (d) Liu J, Kvetny M, Feng J, Wang D, Wu B, Brown W, Wang G. Langmuir. 2012; 28:1588. [PubMed: 22182684]
27. Newman, J.; Thomas-Alyea, KE. Electrochemical Systems. John Wiley & Sons; Hoboken: 2004. p. 424
28. Lan W-J, Holden DA, Zhang B, White HS. Anal Chem. 2011; 83:3840. [PubMed: 21495727]

29. Willmott GR, Parry BET. J Appl Phys. 2011; 109:094307.
30. Myland JC, Oldham KB. J Electroanal Chem. 1993; 347:49.
31. Vogel R, Willmott G, Kozak D, Roberts GS, Anderson W, Groenewegen L, Glossop B, Barnett A, Turner A, Trau M. Anal Chem. 2011; 83:3499. [PubMed: 21434639]
32. Firnkes M, Pedone D, Knezevic J, Doblinger M, Rant U. Nano Lett. 2010; 10:2162. [PubMed: 20438117]
33. White, HS. private communication.
34. Krishnan S, Mani V, Wasalathanthri D, Kumar CV, Rusling JF. Angew Chem, Int Ed. 2011; 50:1175.
35. (a) Aslan K, Perez-Luna VH. Langmuir. 2002; 18:6059.(b) Aslan K, Luhrs CC, Perez-Luna VH. J Phys Chem B. 2004; 108:15631.
36. Aslan K, Perez-Luna VH. J Fluoresc. 2004; 14:401. [PubMed: 15617382]

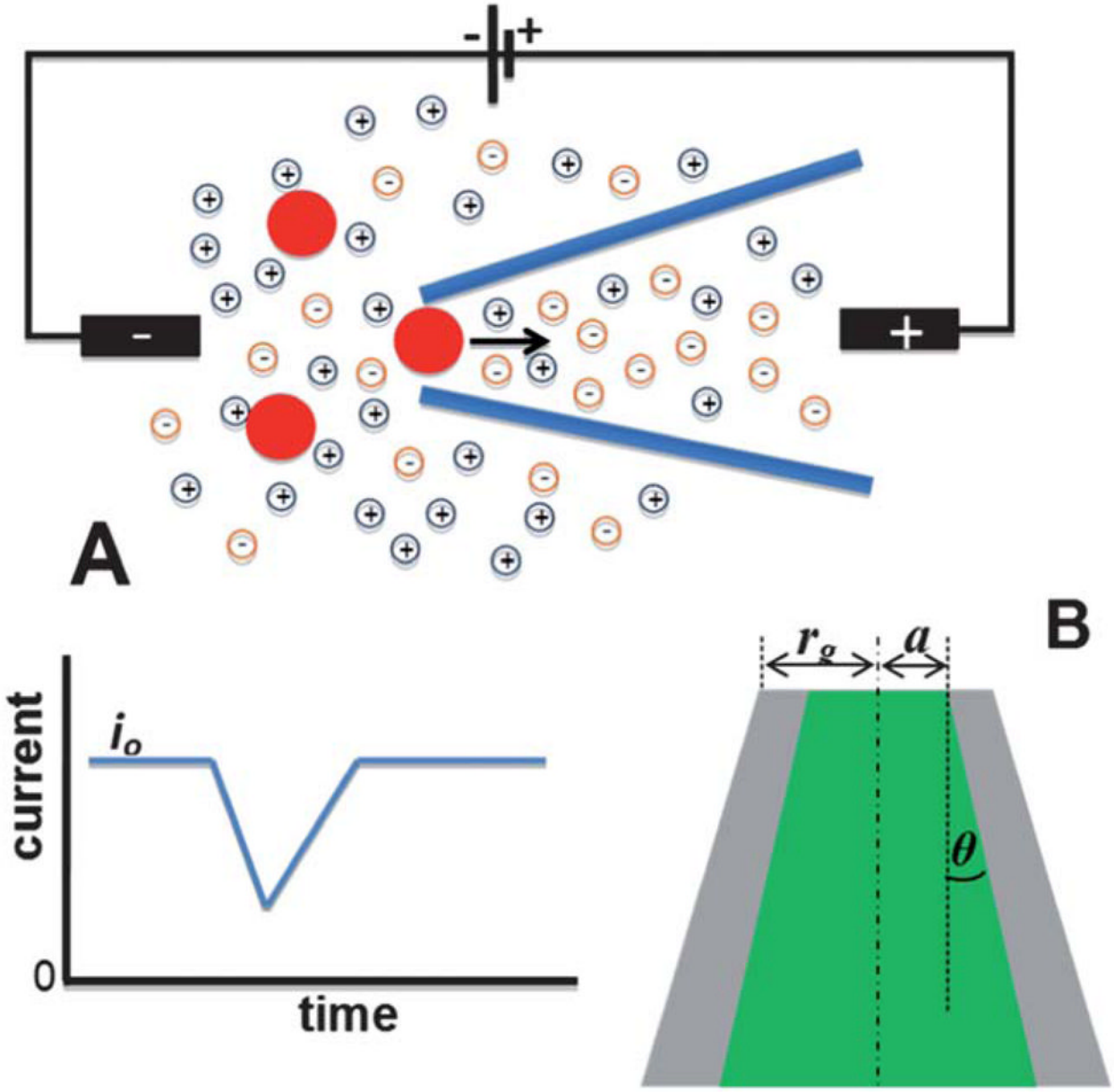

Fig. 1.
(A) Simplified schematic representation of resistive-pulse sensing with a nanopipette. In the presence of nanoparticles, blockage events can be seen in the current *vs.* time curve. (B) Parameters defining the nanopipette geometry.

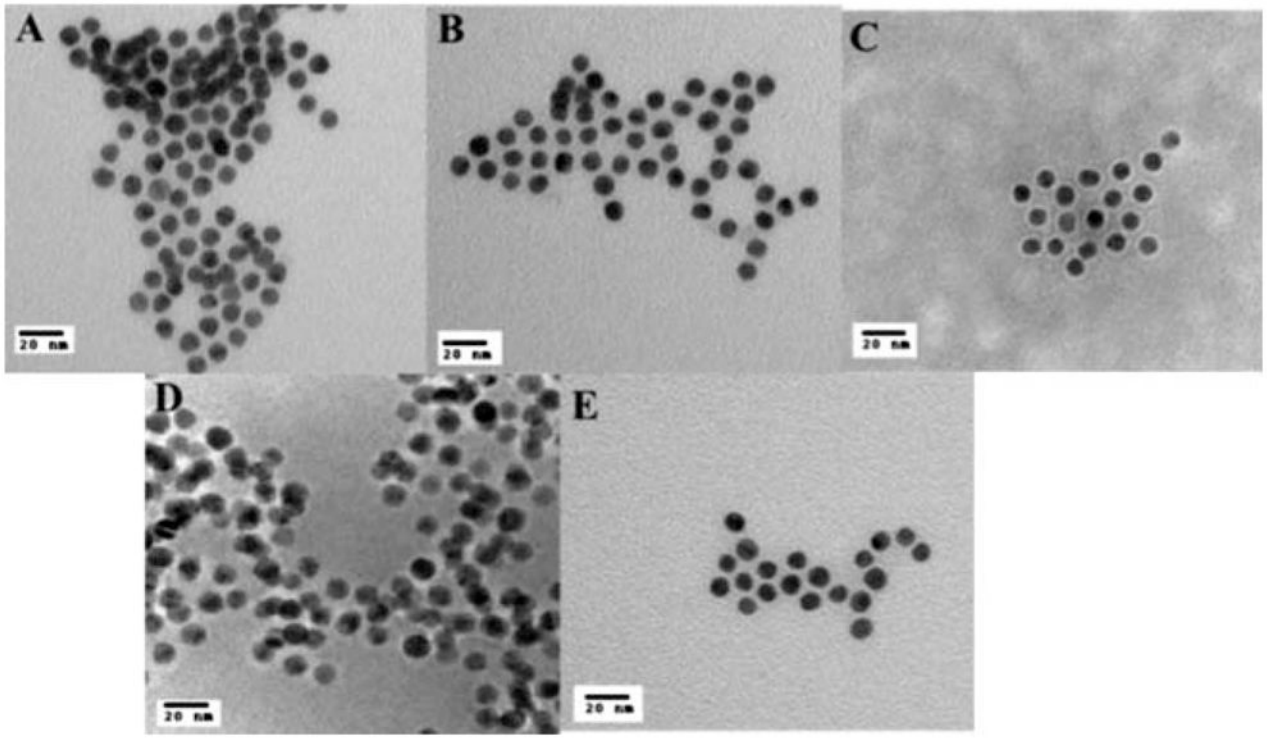

Fig. 2.
TEM images of different nanoparticles: (A) commercial AuNPs, (B) AuNP–MHDA, (C) AuNP–peptide stained by phosphotungstic acid, and (D) Au–peptide–IgY stained by phosphotungstic acid. (E) Control particles: commercial AuNPs stained by phosphotungstic acid.

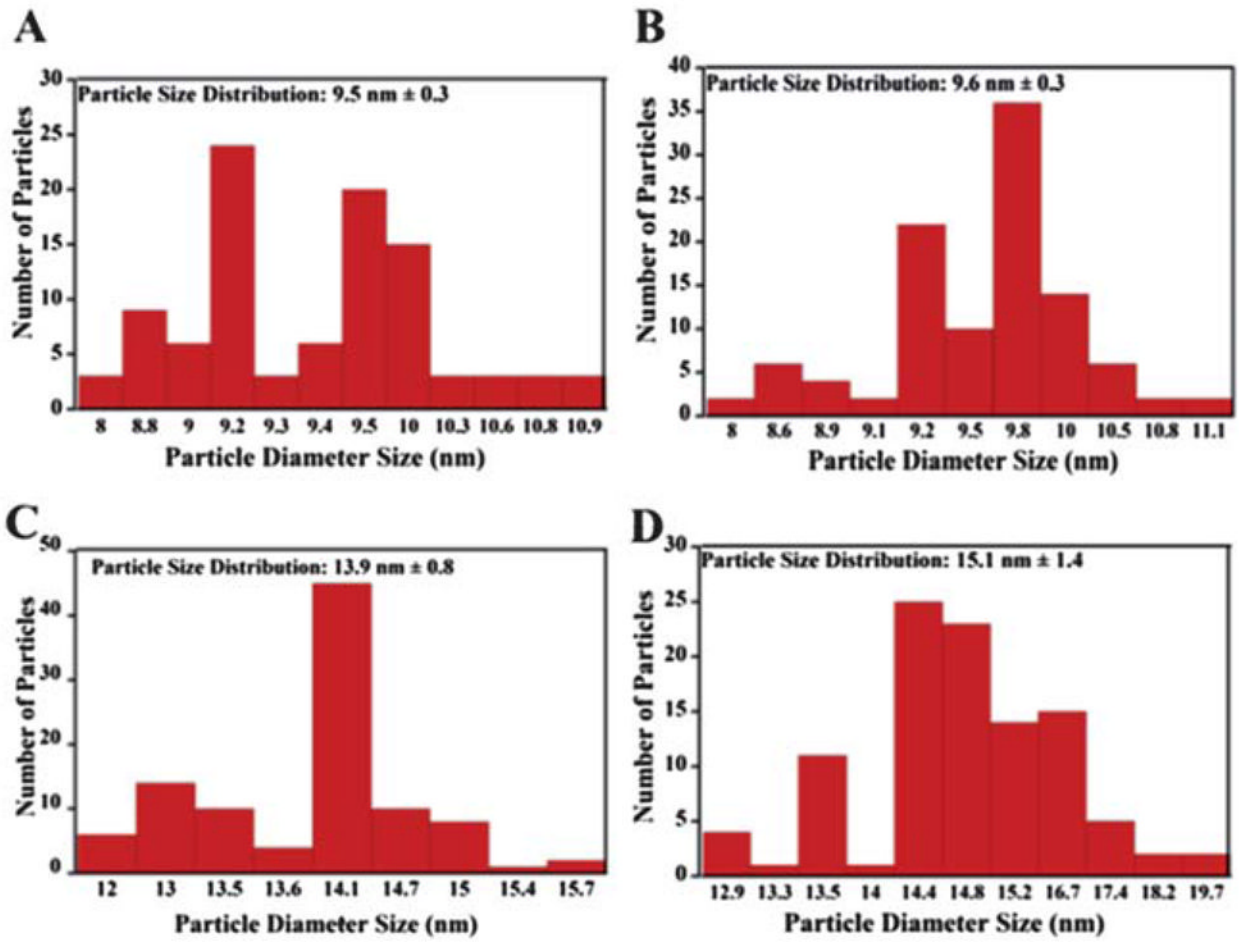

Fig. 3.

Particle size distribution of 110 nanoparticles for (A) commercial AuNPs, (B) AuNP–MHDA, (C) AuNP–peptide, and (D) Au–peptide–IgY.

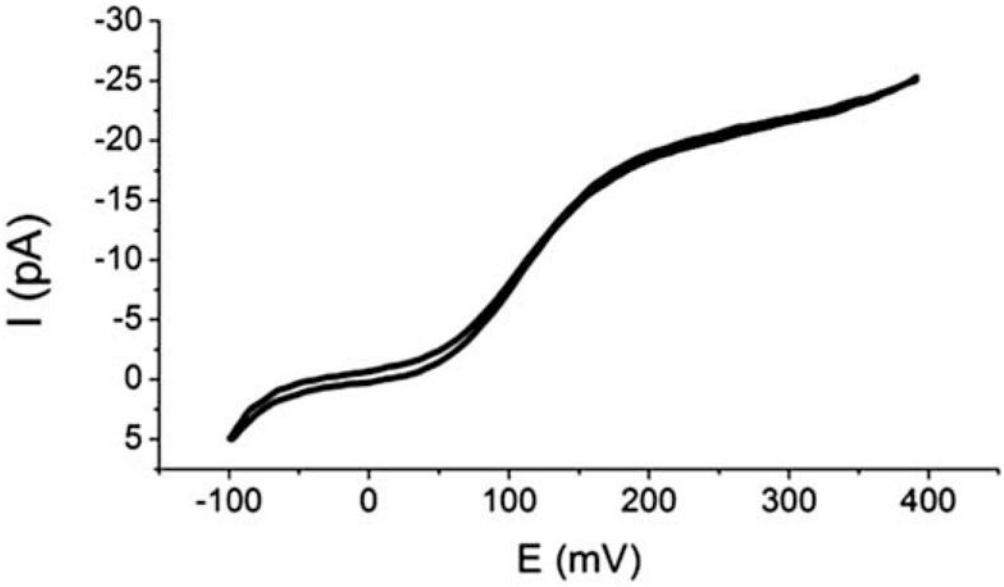

Fig. 4.

Steady-state voltammogram of ClO_4^- transfer across the DCE–water interface obtained with a 25 nm-radius pipette in cell 1 with the potential sweep rate of 50 mV s^{-1}.

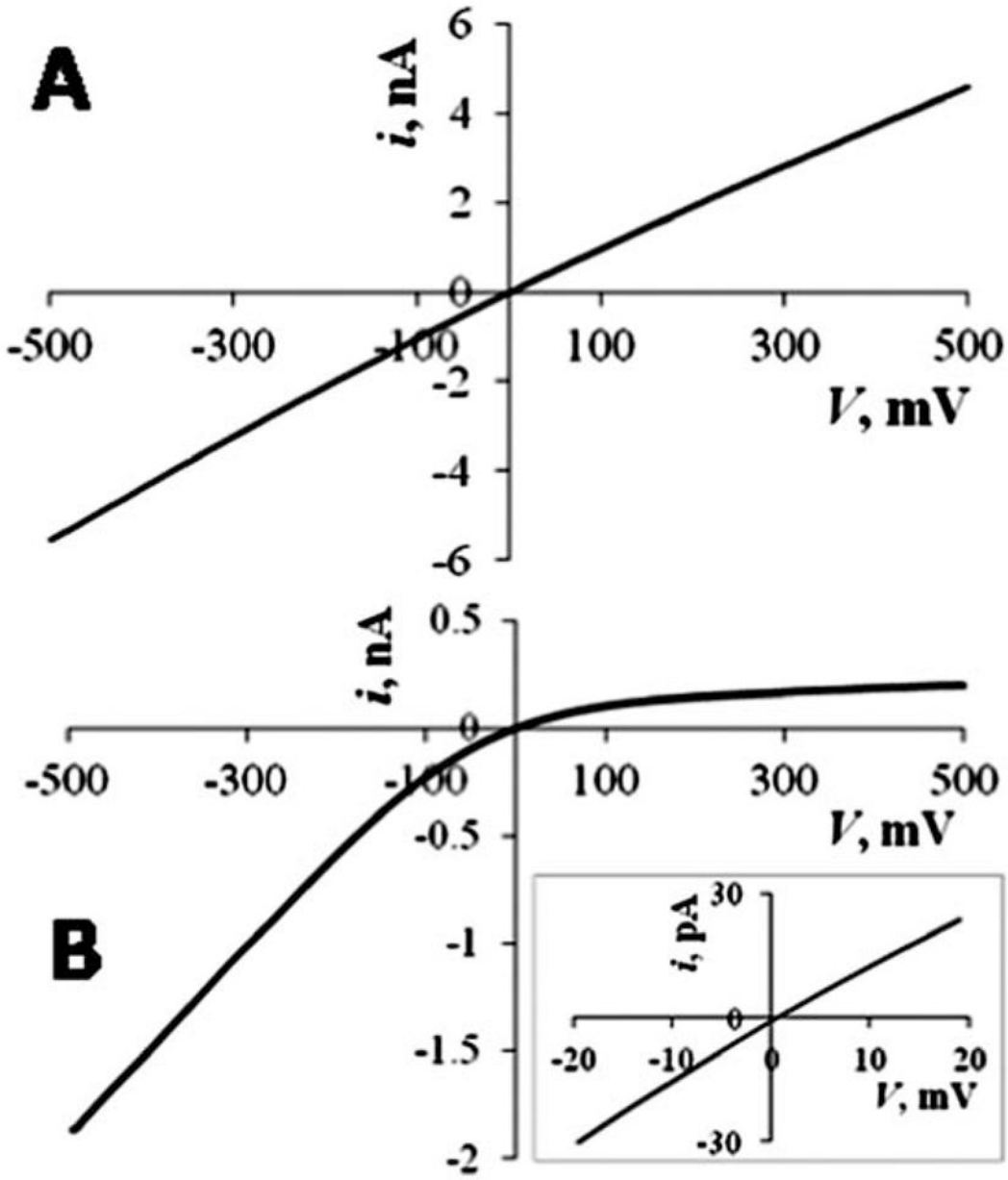

Fig. 5.

i–*V* curves obtained for nanopipettes in 15 mM NaCl + 10 mM PBS (pH 7) *a*, nm =103 (A) and 12 (B). The inset in B shows the linear part of the *i*–*V* curve.

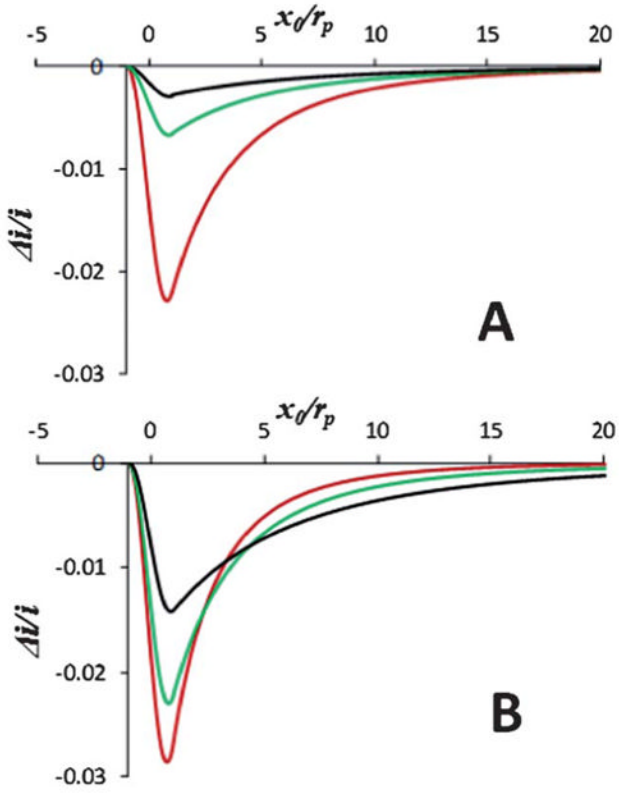

Fig. 6.

Calculated change of current over normalized transferred distance for (A) different r_p/a values: 1/2 (red), 1/3 (green), and 1/4 (black), and θ=10°; and (B) different θ: 5° (black), 10° (green), 15° (red), and r_p/a=1/2.

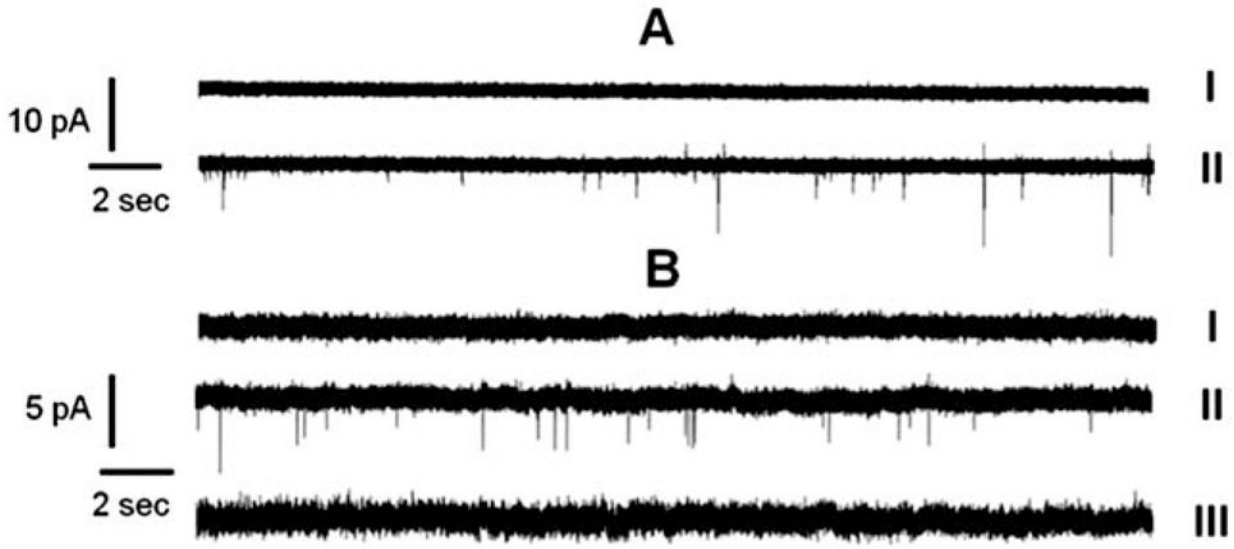

Fig. 7.

Current–time recordings obtained with a (A) 28 nm-diameter and (B) 32 nm-diameter pipette in a 15 mM NaCl + 10 mM PB (pH 7). (A) Solution contained: 0 (trace I) and 2 nM(trace II) of 10 nm-diameter AuNP; V =150 mV. i_0 =156 pA (I) and 134 pA (II). (B) Solution contained: 0 (I) and 1.8 nM (II, III) of AuNP–peptide. V =100 mV (I, II) and −100 mV (III). i_0 =222 pA (I), 233 pA (II) and −363 pA (III).

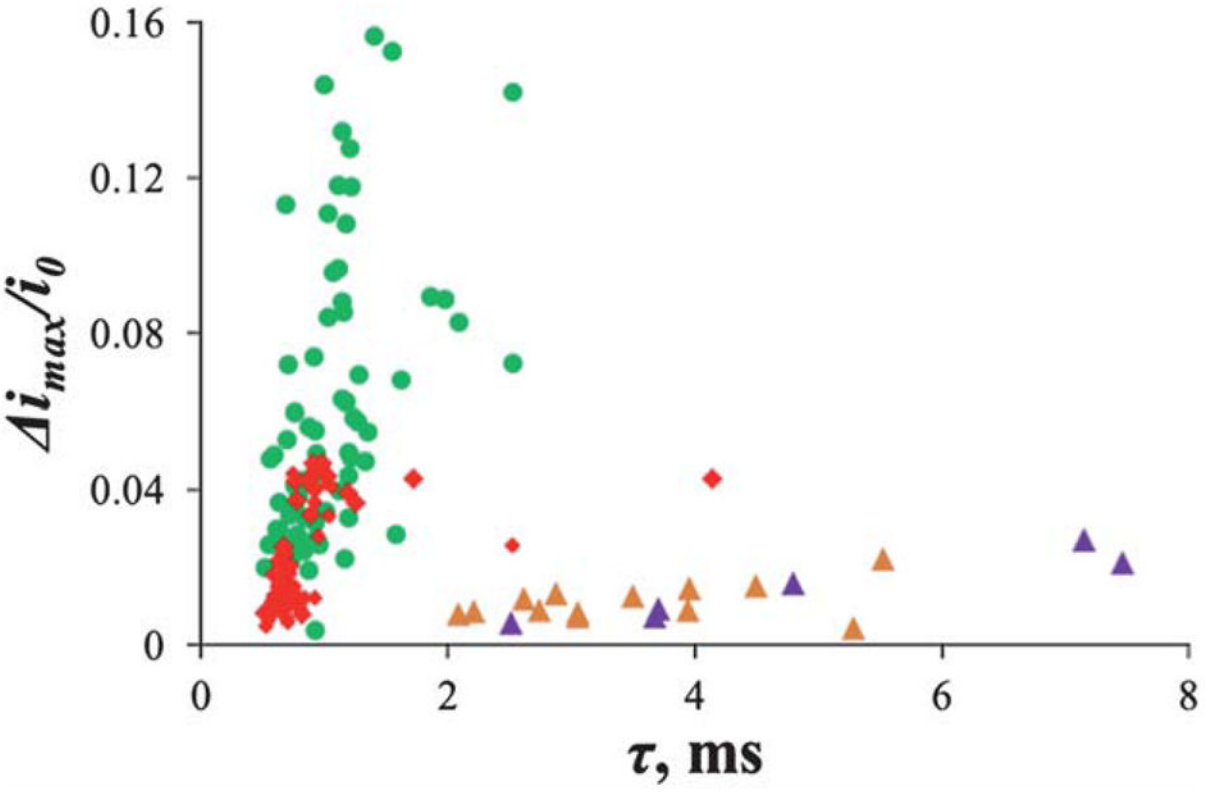

Fig. 8.

Scatter plots of the normalized maximum current change *versus* peak width for AuNP–peptide translocation experiments with three different pipettes. Pipette diameter (nm): 108 (triangles) 28 (diamonds), and 22 (circles). The applied voltage (mV) was: 200 (green; total recording time 24.3 min), 300 (red; 40 s), 800 (purple; 8 min) and 900 (orange; 15.3 min). For other parameters, see Fig. 7.

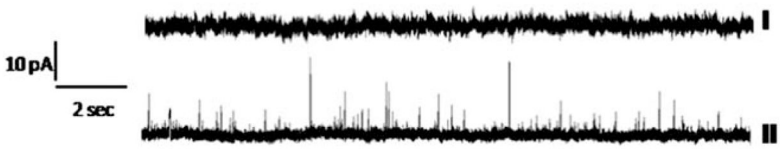

Fig. 9.

Current–time recordings for a 28 nm-diameter pipette in a 15 mM NaCl + 10 mM PB (pH 7) solution containing (I) 0 and (II) 1 nM of Au–peptide–IgY particles. V =−200 mV. i_0 =−655 pA (I) and −545 pA (II).

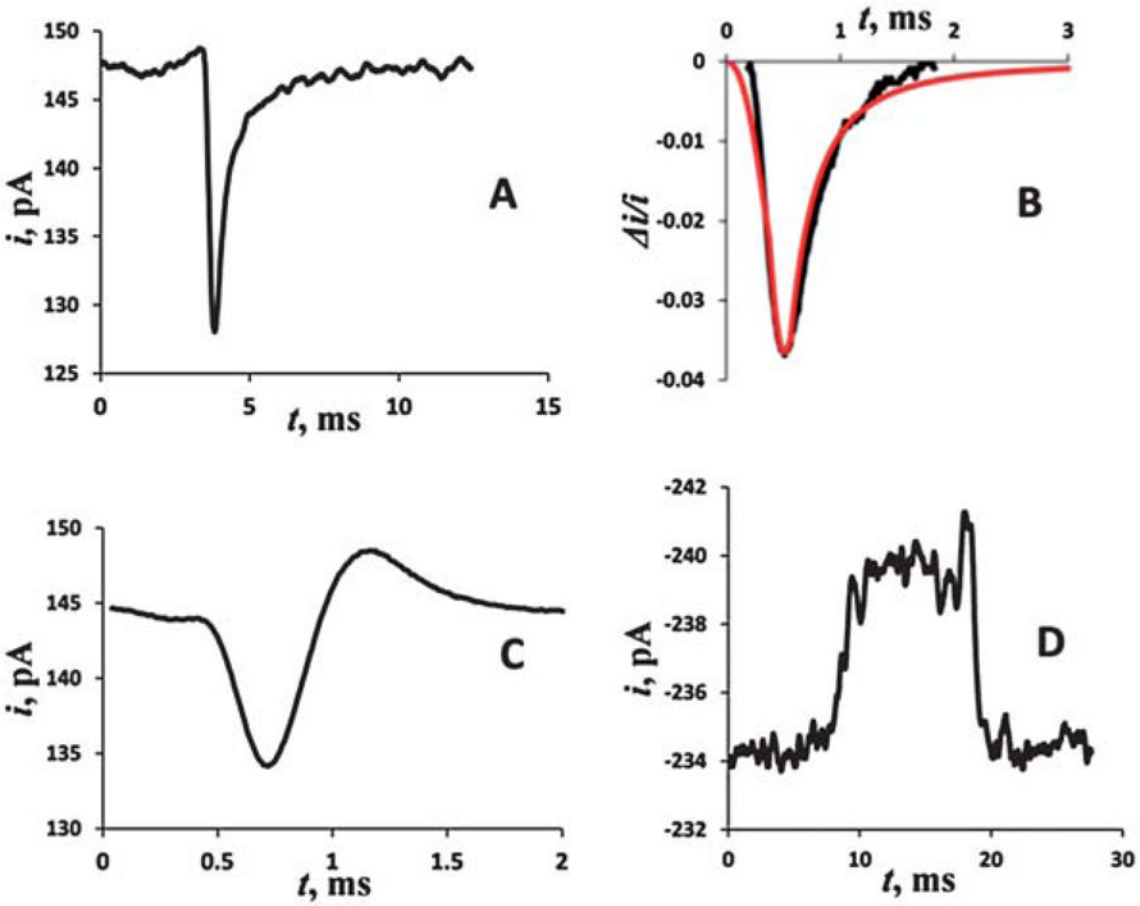

Fig. 10.

Current pulses obtained in solutions containing (A and C) AuNP–peptide, (B) Au–MHDA, and (D) AuNP–peptide–IgY. (B) Experimental (black) and theoretical (red) current–time pulses for the translocation of a Au–MHDA through a 34 nm-diameter pipette.

Table 1

ζ-potentials of different nanoparticles

Particle	ζ-potential	Solution
Citrate-stabilized AuNP	−52 mV	10 mM PB (pH 7) + 15 mM NaCl
AuNP–MHDA	−4.9 ± 2.9 mV	10 mM PB (pH 7) + Tween-20
AuNP–peptide	−32.3 ± 1.1 mV	10 mM PB (pH 7)
AuNP–peptide–IgY	−25.4 ± 0.4 mV	10 mM PB (pH 7)

Table 2

Geometric parameters and resistances of pipettes used in resistive-pulse experiments

a, nm	*R*, GΩ	*θ*,°
11	1.05	5.8
12	0.80	7.1
14	0.60	8.2
17	0.55	7.3
54	0.027	11.0